

Rotary Travelling Wave Oscillator Arrays: - A New Clock Technology

John Wood, Terry C. Edwards *Member IEEE*, Steve Lipa, *Student Member IEEE*

Abstract - Rotary Traveling Wave Oscillators (RTWOs) represent a new transmission-line approach to gigahertz-rate clock generation. Using the inherently stable LC characteristics of on-chip VLSI interconnect, the clock distribution network becomes a low-impedance distributed oscillator. The RTWO operates by creating a rotating traveling wave within a closed-loop differential transmission line. Distributed CMOS inverters serve as both transmission-line-amplifiers and latches to power the oscillation and ensure rotational lock. Load capacitance is absorbed into the transmission-line constants whereby energy is recirculated giving an adiabatic quality. Unusually for an LC oscillator, multi-phase (360°) square waves are produced directly. RTWO structures are compact and can be wired together to form Rotary Oscillator Arrays (ROAs) to distribute a phase-locked clock over a large chip. The principle is scalable to very high clock frequencies. Issues related to interconnect and field coupling dominate the design process for RTWOs. Taking precautions to avoid unwanted signal couplings, the rise and fall times of 20ps, suggested by simulation, may be realized at low power consumption. Experimental results of a 0.25- μm CMOS test chip with 950MHz and 3.4GHz rings are presented indicating 5.5pS jitter and 34dB power supply rejection ratio (PSRR). Design errors in the test chip precluded meaningful rise and fall time measurements.

Index Terms- Clocks, MOSFET oscillators, phase locked oscillators, phased arrays, synchronization, timing circuits, transmission line resonators, traveling wave amplifiers

I. INTRODUCTION

Clocking at gigahertz rates requires generators with low skew and low jitter to avoid synchronous timing failures. The notion of a "clocking surface" becomes untenable at gigahertz rates [1] frequently mandating that large VLSI chips are sub-divided into multiple clock domains and/or utilise skew-tolerant multiphase circuit design techniques [2].

Techniques such as distributed PLL [3] and DLL [4] can control systematic skew to within ± 20 ps but are complex, introduce random skew (i.e. jitter) and have area penalties. H-tree distribution systems while simple, are difficult to balance and can use upwards of 30% of a chip's total power budget [5]. All these systems are inherently single-phase, induce large amounts of simultaneous switching noise and can be highly susceptible to this noise.

Researchers have therefore looked to alternative oscillator mechanisms for better phase stability and lower power consumption. Previous transmission-line systems such as salphasic distribution [6], distributed amplifiers [7] and adiabatic LC resonant clocks [8] provide only a sinusoidal or semi-sinusoidal clock, making fast edge rates difficult to achieve.

This paper introduces the Rotary Travelling Wave Oscillator (RTWO); a differential LC transmission line oscillator which produces GHz rate, multiphase (360°) square-waves with low jitter. Extension of the RTWO to Rotary Oscillator Arrays (ROAs) offers a scalable architecture with the potential for low power, low skew, clock generation over an arbitrary chip area without resorting to clock domains. Simulations predict rise and fall times of 20 ps on a 0.25- μm process and a maximum frequency limited only by the f_r of the integrated circuit technology used.

Experiments show that although the RTWO operates differentially, careful attention is required to guard against magnetic field couplings between the clock conductors and other structures if the potential performance of these oscillators is to be realised.

II. CONCEPT OF THE ROTARY CLOCK OSCILLATOR

A. Fundamentals and Structures

The basic ROA architecture is shown in Fig. 1. A representative multi-GHz rotary clock layout has 25 interconnected RTWO rings placed onto a 7×7 array grid. Each ring consists of a differential line driven by shunt-connected anti-parallel inverters distributed around the ring. This arrangement produces a single clock 'edge' in each ring which sweeps around the ring at a frequency dependent on the electrical length of the ring. Pulses are synchronized between rings by hard wiring which forces phase lock.

Fig. 2 illustrates the theory behind the individual Rotary Travelling Wave Oscillator. Fig. 2a depicts an open loop of differential transmission line (exhibiting LC characteristics) connected to a battery through an ideal switch. When the switch is closed a voltage wave begins to travel

counterclockwise around the loop. Fig. 2b shows a similar loop, with the voltage source replaced by a cross-connection of the inner and outer conductors to cause a signal inversion. If there were no losses, a wave could travel on this ring indefinitely, providing a full clock cycle every other rotation of the ring (the Möbius effect).

In real applications, multiple anti-parallel inverter pairs are added to the line to overcome losses and give rotation lock. Rings are simple closed loops and oscillation occurs spontaneously upon any noise event. Unbiased, start-up can occur in either rotational sense - usually in the direction of lowest loss. Deterministic rotation biasing mechanisms are possible e.g. directional coupler technology or gate displacement [9]. Once a wave becomes established it takes little power to sustain it, because unlike a ring oscillator, the energy that goes into charging and discharging MOS gate capacitance becomes transmission line energy which is recirculated in the closed electromagnetic path. This offers potential power savings as losses are not related to CV^2f but rather to I^2R dissipation in the conductors where R can be reduced e.g. by adoption of copper metallization.

B. Waveforms

Fig. 3 shows simulated waveforms of a 3.4GHz RTWO taken at an arbitrary position on the ring. The design has the following characteristics for reference:

Conductors: Width = 20 μm , Pitch = 40 μm , Ring Length = 3200 μm , Metallization: 1.75 μm copper, Loop inductance total = 1.87 nH. Process: 0.25- μm CMOS. Nch total width: 2000 μm , Pch total width: 5000 μm . Number of inverters: 24 pairs.

Very large distributed transistor widths give substantial capacitive loading to the lines, thus lowering velocity to give a reasonably low clock rate from a compact oscillator structure. In application, upto 75% of this capacitance can come from load capacitance, reducing the size of the drive transistors accordingly.

The upper traces of Fig. 3 show the simulated voltage waveforms on the differential line at points labeled A0, B0. The lower traces show the current in the conductors to be ± 200 mA, while the supply current is simulated at 84 mA with ± 4.5 mA of ripple. This clearly illustrates that energy is recycled by the basic operation of the RTWO. Just driving the 34pF of capacitance present would require 275mA at this frequency (from CVf).

C. Phase Locking

Interconnected rings, as in Fig. 1a, will run in lock-step, ensuring that the relative phase at all points of a ROA are known. It is possible to use a large array of interconnected rings to distribute a clock signal over a large die area with low clock skew. For example, referring to Fig. 1a, all the points marked with the equals sign (=) have the same relative phase as that arbitrarily marked as 0° . At any point along the loop, the two signal conductors have waveforms 180 degrees out of phase (2-phase non-overlapping clock). A full 360 degrees is measured along the complete closed path of the loop. In principle, an arbitrary number of clock phases can be extracted. Phase advances or retards depending on the direction of rotation and Fig 4. shows the current / voltage relationships for clockwise and counter-clockwise rotation.

D. Network rules

Although the square ring shape is convenient to show diagrammatically it is only one example of a more general network solution which requires ROAs to conform closely to the following rules:

- (i) Signal inversion must occur on all (or most) closed paths.
- (ii) Impedance should match at all junctions.
- (iii) Signals should arrive simultaneously at junctions.

From (i) above, any *odd number* of crossovers are allowed on the differential path and regular crossovers forming a braided or "twisted pair" effect can dramatically reduce the unwanted coupling to wires running alongside the differential line.

The differential lines would typically be fabricated on the top metal layer of a CMOS chip where the 'reverse scaling' trend of VLSI interconnect offers increasingly high performance [10].

E. Fields and currents

Figure 5 illustrates a three-dimensional section of the ring structure connected to a pair of CMOS inverters expanded to show the four individual transistors. The main current flow in the differential conductors is shown by solid arrows, the magnetic field surrounding these conductors by dashed loops and the capacitance charge / signal-boost current flowing through the transistors by dashed lines.

An important feature of differential lines is the existence of a well-defined "go" and "return" path which gives predictable inductance characteristics in contrast to the uncertain return-current path for single-ended clock distribution [11].

Capacitance arises mainly from the transistor gate and depletion capacitance and interconnect capacitance does not dominate.

R_{gi} indicates "Intrinsic Gate Resistance" i.e. the ohmic path through which the gate charge flows. The term R_{gi} implies a parasitic gate term but in reality most of this resistance is in the series circuit of the channel under the gate electrode. This is shared by the D-S channel as illustrated by the triangular region (shown with transistors operating in the pinch-off region).

F. Coherent Amplification, Rotation Locking

Figure 6 is an expanded view of a short section of transmission line with three sets of back-to-back inverters shown. It is assumed that start-up is complete and the rotating wave is sweeping left to right. For this analysis we view the inverter pairs as discrete latch elements.

Each latch switches in turn as the incident signal, travelling on the low impedance transmission line, overrides the "on" resistance of the latch and its previous state. This "clash" of states occurs only at the rotating wavefront and therefore only one region is in this cross-conduction condition at any one time. The transmission-line impedance is of the order of 10Ω and the differential on-resistance of the inverters is in the 100Ω to $1\text{ k}\Omega$ range depending on how finely they are distributed throughout the structure.

Once switched, each latch contributes for the remainder of the half cycle, adding to the forward-going signal. Coherent build-up of switching events occurs in this forward direction only. An equal amount of energy is launched in the reverse direction but the latches in that direction cannot be switched further into the state to which they have already switched. The reverse-travelling components simply reduce the amount of drive required from those latches.

Importantly, it is the non-linear latching action which is responsible for the self-locking of direction (a highly linear amplifier has no such directionality).

To clarify the above statements, Fig. 7 demonstrates how a large CMOS latch responds to an imposed differential signal. The curve trace shows a central, differential-amplification region bounded by two absorptive ohmic regions (shaded) corresponding to the two latched states.

Except at the wavefront location where amplification takes place, the ring structures will be terminated ohmically to the supplies.

The four-transistor 'full-bridge' circuit minimises supply current ripple to the cross-conduction period.

G. Frequency and Impedance relations

In simulation models (and indeed as fabricated), the RTWO transmission-line is built up from multiple R,L,C segments and therefore these primary line constants must be identified.

Fig. 8a is the basic RF macromodel of a short length (*SegLen*) of RTWO line with all significant RF components and parasitics annotated (as per Fig.5). Suffixes identify per-unit-length *perlen*, lumped *lump* and *total* (or *loop*) values. There are *Nseg* segments connected together, plus a crossover, to produce a closed ring of length *RingLen*.

Fig. 8 (b) is a capacitive equivalent circuit for the transistor and load capacitances. AC0 indicates an AC ground point (*VDD* and *VSS*).

The differential lumped capacitance C_{lump} of one such segment is given approximately by

$$C_{lump} = C_{AB\ int} + C_{dgN1} + C_{dgN2} + C_{dgP1} + C_{dgP2} + (C_{gsN1} + C_{gsN2} + C_{dbN1} + C_{dbN2} + C_{gsP1} + C_{gsP2} + C_{dbP1} + C_{dbP2} + C_{loadA} + C_{loadB})/4 \quad (1)$$

where:

$C_{AB\ int}$ = the interconnect capacitance for the line AB

C_{dg} = the gate overlap and Miller-effect feedback capacitance

C_{gs} = total channel capacitance

C_{db} = drain depletion capacitance to bulk (substrate)

C_{load} = load capacitance added to a line.

(Note that the /4 is used to convert the in-parallel "to ground" values into in-series differential values of capacitance)

$C_{AB\ int}$ is usually a small part of total capacitance and accurate formulas are available [12] if needed.

To calculate the per-unit-length differential inductance i.e. accounting for mutual coupling we use [13].

$$L_{perlen} = \left(\frac{\mu_o}{\pi} \right) \log \left\{ \left(\frac{\pi \cdot s}{w + t_c} \right) + 1 \right\} \quad (2)$$

where: s = conductor separation w = conductor width t_c = conductor thickness

The phase velocity is given by:

$$v_p = \frac{1}{\sqrt{L_{perlen} C_{eff,perlen}}} \quad (3)$$

where

$$C_{eff,perlen} = \frac{Clump}{SegLen}$$

For heavily loaded RTWO structures, V_p can be as low as 0.03 of c (where c is the free space velocity i.e. 2.998×10^8 m/s)

The clock frequency f_c is given approximately by the expression

$$f_c = \frac{V_p}{[2 \cdot RingLen]} \quad (4)$$

(The x2 factor arises from the pulse requiring two complete laps for a single cycle)

Differential characteristic impedance is given by

$$Z_0 = \sqrt{\frac{L_{perlen}}{C_{eff,perlen}}} \quad (5)$$

Transmission line characteristics dominate over RC characteristics when [14]:

$$R_{loop} < 2Z_0 \quad (6)$$

H. Bandwidth and power consumption

Seen from an RF perspective, Fig.8a shows the RTWO to be two push-pull distributed amplifiers folded on top of each other. Distributed amplifiers exhibit very wide bandwidth because parasitic capacitances are "neutralised" by becoming part of the transmission-line impedance [15]. Performance is limited by the carrier transit time of the MOSFETs [16], not by the traditional digital inverter propagation time t_{pd} which is not applicable where gates and drains

are driven co-operatively by an imposed low-impedance signal and where the load capacitance is hidden in the transmission-line.

Operation of RTWO is largely adiabatic when the voltage drop required to charge the capacitances is developed mainly across the inductance:

$$Z(L_{lump}) \gg R_{seg} \quad (7)$$

and when the intrinsic gate resistance is low relative to the reactance of the gate capacitance.

$$R_{gi} \ll Z(C_{gate}) \quad (8)$$

RTWO rise and fall times are controllable by setting the cut-off frequency of the transmission lines.

$$f_{cutoff} = \frac{1}{2\pi\sqrt{L_{lump}C_{lump}}} \quad (9)$$

Edges become faster and cross-conduction losses are reduced when the structure more distributed.

The table below lists characteristic changes with N_{seg} where $L_{lump} = L_{total} / N_{seg}$, $C_{lump} = C_{total} / N_{seg}$ with L_{total} and C_{total} held constant.

Table 1 Changes of characteristics with N_{seg} .

Number of Segments N_{seg}	Clock Frequency f_c GHz	Cutoff frequency f_{cutoff} GHz	Rise/Fall ps	Supply Current mA
8	3.25	8.6	50	100
24	3.38	25.9	25	87
72	3.44	77.6	<15	78

The most significant power loss mechanism for RTWO is I^2R power dissipated in the interconnect given by:

$$P_{disp} = \frac{V_{DD}^2}{Z_0^2} R_{loop} \quad (10)$$

Most of the remaining losses in Table1 above are attributed to cross-conduction and parasitic R_{gi} losses. R_{gi} is a real loss mechanism for GHz signals and RTWO rise/fall times can be doubled by this phenomenon. In newer CMOS processes R_{gi} improves with shorter channel length.

III. MORE DETAILED CONSIDERATIONS

A. Skew Control.

Interconnected RTWO loops offer the potential to control skew in spite of relatively large 'open-loop' time-of-flight mismatches. Functionally, phase averaging occurs by pulse combination at the junction of multiple transmission lines. For a 4-port junction, the normal operating mode will see two pulses arriving at the junction simultaneously. These two sources will feed two output ports and signal flow will be unimpeded by reflections if impedance is matched. This amounts to a situation similar to that described in [17][18] although for ROAs the mechanism is LC transmission-line energy combination, not ohmic combination of CMOS inverter outputs.

Where there exists a time-of-flight mismatch, one pulse arrives at the junction before the other. Fig 9a depicts the operation of a 4-port junction between of two inter-wired but velocity-mismatched RTWO loops. Each of these rings has been divided into segments numbered 0..23 (each as Fig8). Four rings are wired together (similar to Fig16 shown later). Only the junction of the rings $x_{0,y1}$ and $x_{1,y2}$ are considered here; the latter having a higher 'open-loop' operating frequency.

From simulation, two pulse-combination effects appear to be present, the simplest of which is the impedance match effect where the first signal to arrive at a junction must try to drive three transmission lines. If all ports have equal impedance, the junction can only reach a quarter of the full signal value and a reflection occurs driving an inverted signal back down the incident port (Fig. 9b). Initially detrimental effects on signal fidelity arising from this reflection are overcome when the other pulse arrives whereupon the pulses combine and branch into the output ports as shown in Fig 9c.

The second pulse combination effect is believed to be due to non-linear MOSFET drain capacitance which can modulate the velocity of the line. Reflections can drive the MOSFETS from the ohmic state into the low-capacitance pinch-off region, locally increasing velocity.

Quantitative results from simulation:

Fig 10 presents the results of a SPICE simulation of the above situation with an extreme condition of velocity mismatch. A +50% variation of T_{ox} oxide thickness is modelled across a small 2.4x2.4mm chip having four interconnected rings. Thick oxide (lower C) devices are on the right side of the chip giving a 22.5% phase velocity increase relative to the left side.

Looking at these results with reference to (Fig.9) reveals that the first pulse arrives from ring (x_1, y_2) and passes point A18_{x1,y2} at time $t_0 + 25$ ps and begins its rise time. Within this rise time the leading edge reaches the nearby junction where negative reflections bounce back to momentarily prevent A18_{x1,y2} passing through the 1.5volt level.

The second pulse arrives from the slower left-hand ring (x_0, y_1) , reaching point B6_{x0,y1} at approximately $t_0 + 45$ ps. It then combines with first pulse at the junction to branch into the two output ports without further reflections.

By $t_0 + 75$ ps, the signals have reached points A16_{x1,y2} and B4_{x0,y1} and are essentially coincident - forward progress of the waves in rings (x_0, y_1) and (x_1, y_2) are now synchronised.

The phase locking phenomenon occurs at every junction of the array (not just the junction considered here) and twice per oscillation cycle which accounts for the smaller than expected initial skew seen between the rings.

Simulations of typical arrays show that lock-up is achieved within a few ns from power-up after signals settle into the 'lowest-energy' state of coherent mesh.

B. Coupling Issues related to layout.

The induced magnetic fields from the Rotary Clock structures can be strong. This is because $\partial I / \partial t$ is relatively high (square waves). The magnetic coupling coefficient however, depends on the angle between source and victim and falls to zero when the angle becomes 90°.

Fig. 11 illustrates a 90° layout technique to minimise inductive coupling problems. The top metal M5 (running left to right) is used to create the differential RTWO while orthogonal M4 is used as a routing resource for busses into and out of areas bounded by the clock transmission-line.

For capacitive coupling, fast rise and fall times imply high displacement currents and a potentially aggressive noise source. Differential transmission lines tend to mitigate such effects [19] and in (Fig. 11) the total capacitive coupling area between each of the transmission-line conductors and any M4 conductor is balanced. If the clock source were ideally differential, no net charge would be coupled to the M4 wires. For the RTWO, distributed inverters force the waveforms to be substantially differential and non-overlapping keeping glitches below the sensitivity of a typical gate.

For the five-metal test chip (Section V), a 45% utilization of M4 was used for the 90° routing pattern immediately underneath the RTWO rings. This coverage allows the M4 to act as both a

routing resource and as an electrostatic shield similar to [20] preventing electrostatic coupling to signal lines further below. Magnetic fields are not attenuated much by this configuration because the spaces between the thin perpendicular M4 lines break up the circulating currents which could repel a magnetic field. Substrate magnetic fields [21] are therefore to be expected.

Coupling to co-parallel (0°) victim conductors is potentially much more problematic (discussed later in section IV C. "Coupling II - simulated coupling").

C. Tap-off Issues and stub loadings..

It is possible to "tap into" the ROA structure (Fig.11) anywhere along its length and extract a locally two-phase signal with known phase relationship to the rest of the network. This signal can then be routed via a fast differential transmission-line to other circuits and will generally represent a capacitive stub on the RTWO ring.

For minimum signal distortion, the round-trip time-of-flight τ_p (forwards and backwards along the stub) must be much less than the rise-time τ_r and fall-time τ_f of the clock waveform:

$$\tau_p \ll \tau_r, \tau_f \quad (11)$$

When the above condition is met, the capacitance can be taken as being effectively lumped on the main RTWO ring at the tap point for the purposes of predicting oscillator frequency and ring impedance.

Although not immediately apparent, this condition is achievable in practice due to three factors. The first factor is that the tap line velocity is relatively fast for SiO_2 dielectric it is approximately $0.5c$ while the main RTWO oscillator ring might be operating at perhaps $0.075c$. The second factor is that the tap length only has to be long enough to reach within a single RTWO ring. The third factor is that it requires two signal rotations on the RTWO to complete a clock cycle. These three factors work together to make the RTWO rings physically small compared to the expected speed-of-light dimensions. The distances to be spanned by the fast tap wires are therefore short enough that transmission-line effects on these lines are unimportant - certainly at the clock fundamental frequency and even at higher harmonics.

This can be illustrated by reference to a specific 3.4 GHz RTWO, $3200\mu m$ long with 20ps rise/fall times. Within one of these rise or fall periods a stub transmission-line with velocity $0.5c$ is able to communicate a signal over a distance of 3mm. For a stub length of $400\mu m$ (to reach the centre of the ring) this equates to 3.75 round-trip times along the stub.

Fig 12 shows simulated waveforms with 2pF of total to-ground capacitance at the end of one such stub. Reflected energy gives rise to the ringing which is evident with this level of capacitance. The line resistance of the stubs must be low to maintain reflective energy conservation.

The ratiometric factors outlined above between ring length, frequency, rise/fall time and stub lengths are expected to hold as ROAs are scaled to higher frequencies and smaller ring lengths without requiring special stub tuning measures.

Capacitive loading limits

Substantial total-chip capacitive loading can be tolerated by RTWO relative to conventionally resonant systems [8][22][23]. However, the loading effects of interconnect, active and stub capacitances cannot be increased without limit. The consequential lowering of line impedance increases circulating currents until I^2R losses become a concern. Eventually the impedance becomes so low relative to the loop resistance that the relation (6) cannot be maintained and whereupon oscillation ceases altogether.

D. Frequency / Impedance Adjustment

Rewriting equation (4) in the form below shows that frequency is set only by the total inductance and capacitance of the RTWO loop.

$$f_{osc} = \frac{1}{2\sqrt{L_{total}C_{total}}} \quad (12)$$

Total loop inductance, L_{total} is proportional to *RingLen* and varies strongly as a function of the width and pitch of the top metal differential conductors. This allows a coarse frequency selection through the top-metal mask definition. Unit-to-unit inductance variation is expected to be small because of the good lithographic reproduction of the relatively large clock conductors and the weak sensitivity of inductance to metal thickness variations.

Total capacitance, C_{total} for RTWO is the sum of all lumped capacitances connected to the loop (equation 1). C_{total} tends to be dominated by gate oxide capacitance (C_{ox}) from the drive FETs and the clock load FETs. C_{ox} is inversely proportional to gate oxide thickness T_{ox} which on a modern CMOS SiO_2 is controlled to approximately $\pm 5\%$ variation over extended wafer

lots [24]. Drain depletion capacitances exist on bulk CMOS where the active transistors connect to the ring.

During the VLSI layout phase, a CAD tool (expected release: Q1 2002) can target a fixed operating frequency. The tool will be able to correct impedance discontinuities caused by lumped load capacitance by the addition of dummy "padding" capacitance elsewhere around the loop, and post-compensate an overly capacitive-loaded clock network by reducing the differential inductances through pitch reduction - hence restoring velocity and thus frequency. Alternatively, at the expense of using more metallization, a new layout with more numerous, shorter length rings could be used. The tool will need to simultaneously solve impedance matching issues (refer to section II A, Equation (5)). By manipulation of both L and C simultaneously, it is possible to control v_p and Z independently as shown diagrammatically in Fig. 13. For example velocity v_p can be reduced by increasing both L and C by the same factor to cancel the effect on Z . These adjustments can support arbitrary branch-and-combine networks (at least in theory).

Post fabrication, adding together the sources of variation and given that frequency is related to \sqrt{C} and \sqrt{L} , a $\pm 5\%$ initial tolerance of operating frequency between parts is expected. Matching within a die should be better, but temperature gradients and transistor size variations as they affect capacitance will lead to phase velocity changes requiring correction by the *Skew Control* mechanism described in (section III A).

Temperature can alter frequency through variation of L_{total} and C_{total} . Inductance variation is assumed to be negligible compared to capacitance variation and is not considered. Gate oxide thickness variation could potentially affect C_{total} but for SiO_2 dielectric, with properties similar to quartz, this can be ignored. More significant are temperature variations of drain depletion capacitance and of transistor L_{eff} , W_{eff} .

To tune an ROA clock to an exact reference frequency, allowing limited "speed-binning" and reduced internal phase mismatches, closed-loop control of distributed switched capacitors [9] or varactors [25] is envisaged.

E. Active compensation for interconnect losses

Resistive interconnect losses make it difficult to communicate high frequency clock signals over a large chip without waveshape distortion and attenuation which impacts on the practicality

of reflective energy conservation schemes [6][22][23]. The skin effect loss mechanism has been evident in clock tree conductors for some time [26] and is frequency dependent. High speed H-trees tend to use hierarchical buffers within the trees to maintain amplitude and edge rates.

Active compensation of VLSI differential transmission-lines to overcome clock attenuation was shown by Bußmann and Langmann [27] to be applicable to sine-wave signals. Shunt-connected negative impedance convertors (NICs) were used with linear compensation to prevent oscillations.

The distributed inverters used within RTWOs afford active compensation for transmission-line losses, raising the apparent Q of the resonant rings and helping to maintain a uniformly high clock amplitude around the structure.

F. Logic Styles.

Two-phase latched logic [28] is the style most compatible with RTWO. It is highly skew tolerant and through dataflow-aware placement [27] offers the potential to exploit the full 360° of clock phase to reduce clock related surging [29] which in future systems could exceed 500A [30]. Conventional single-phase D-latch designs can be driven where timing improvements through skew-scheduling [31] might be possible. A locally 4-phase system to support domino logic [2] could be implemented by wrapping two loops of RTWO line around the region to clock. Unfortunately all of these techniques are beyond the capability of current logic synthesis tools.

IV. SIMULATED PERFORMANCE

A. Approach

To enable rapid "what-if" evaluation of potential RTWO structures, a simulation / visualization program known as "Rotary Explorer" [32] has been developed. Rotary Explorer is GUI driven and parametrically creates a SPICE deck of macromodels linking to FASTHENRY subcircuits [33] for multi-pole magnetic analysis of skin, proximity and LR coupling effects in the time domain. MOSFETs are modelled using BSIM3v3 non-quasi-static model with an external resistor added to model R_{gi} (Fig.8). The BSIM4 model [34] which properly accounts for R_{gi} as a D-S channel component was not available.

With the Rotary Explorer program it is possible to simulate RTWO rings independently or as interlocked X,Y arrays. The effects of tap loads, oxide thickness variations and magnetically induced "victim" noise and can be evaluated.

As a visualization aid, Rotary Explorer gives a "live" display of color-coded SPICE voltages projected onto a scaled image of the ROA structure being simulated. This aids in the intuitive understanding of reflections and how the structure achieves a steady-state, phase locked operation.

B. Results

Two very important performance metrics for any oscillator are its sensitivity to changes in temperature and supply voltage. Simulations of these effects on a nominally 3.34 GHz rotary clock resulted in the following tabulated data:

Table 2 Variations with Temperature

Temperature °C	-50	+25	+150
Clock frequency GHz	3.36	3.34	3.31

Table 3 Variations with DC Supply Voltage V_{DD}

Supply voltage V_{DD}	1.5	2.5	3.5
Clock frequency GHz	3.45	3.34	3.32

Supply induced jitter

Following on from above and in light of the RTWO's time-of-flight oscillation mechanism it is inferred that such voltage sensitivity will also apply to phase modulation vs. voltage, i.e. jitter - at least at low supply-noise frequencies. For a single RTWO ring, the power-supply induced

jitter ϕ will be related to ΔV and the rejection ratio $PSRR$ by $\phi = \Delta V * (PSRR)$ (13) Where

ΔV , because of the distributed nature of the oscillator, is the mean supply voltage deviation as experienced along the path of an edge as it travels two complete rotations.

To improve PSRR, plans are in place to add voltage dependent capacitance to the structure to give first-order compensation.

From simulations we see that jitter reduces for multiple ring structures due to averaging effects.

C. Coupling II - simulated coupling:

The Rotary Explorer program makes it easy to simulate coupled noise between an RTWO ring and user defined 'victim' trace (drawn with the aid of a mouse). Simulated results are tabulated

below for a 3.4 GHz RTWO configured to have 20 ps rise and fall times and with geometry as shown in Fig. 14

Table 4 Induced noise as a function of victim distance and length

<i>Victim Distance μ</i>	<i>Victim Length μ</i>	<i>Noise (approx) mV</i>
17	30	40
	60	60
	120	20
35	30	20
	60	30
	120	10
70	30	10
	60	15
	120	5

Peak coupling magnitude occurs at 60 μm *victim length*. A trace longer than this will see a coupling cancellation effect that approaches zero for each pitch of the 'braiding' it traverses.

Fig 15 illustrates a notably strong coupled signal waveform at *victim distance* = 17 μm , with no loading on the victim trace and one end connected to ground. Note the more sensitive noise scale.

The absolute maximum coupling occurs if *victim distance* is allowed to go to zero. In this case mutual coupling between aggressor and victim is 100% with no cancellation effects from the other differential trace. As a numerical example, it follows that a 2.5volt signal with a rise time of 20ps on a transmission line with a velocity of 0.072 c has the 2.5volt gradient over 430 μm of length (Fig 4 illustrates the concept). Over the 60 μm length discussed above, this equates to 348mV. Slower edge rates, faster transmission-lines and lower supply voltages reduce this figure proportionally.

Long-range inductive noise coupling from the differential transmission line is expected to be small, since (from a distance) the 'go' and 'return' currents are equal and opposite.

Potential problems exist in short-range magnetic coupling to wiring in the vicinity of the clock lines. Inductance is lowered by coupling to any highly conductive structure in which eddy currents can flow to decrease and distort the inducing field. Couplings to less conductive circuits

such as the substrate give a loss mechanism which can be modelled as a shunt term in the transmission-line equations. LC resonance in the small-scale coupled structures is unlikely because of the high resonant frequencies. All of the coupling mechanisms mentioned are edge-rate dependent and this can limit the achievable rise and fall times of RTWO by attenuating the high frequency signal components.

Full RLC layout extraction is essential in the neighbourhood of the clock lines if routing is allowed in these areas. An alternative proposal under investigation is to pre-define a VLSI structure combining clock and power distribution into the same grid to give consistent characteristics and shielding.

V. SOME EXPERIMENTAL RESULTS

Fig. 16 shows a die photograph of a prototype built using a 0.25 μ m 2.5-V CMOS process with 1 μ m Al/Cu top metal M5. The conductors are relatively wide in order to minimise resistive losses of the rather thin M5. The available top-metal area consumed by the transmission-lines was 15%. A general feature of RTWO and ROA is that power can be reduced by increasing the metal area devoted to clock generation. The simple substitution of copper metallization could halve the width of the lines for the same power consumption.

The prototype features a large ring independent of four interconnected smaller rings. The 12000 μ m outer ring uses 60 μ m conductors on a 120 μ m pitch, with 128 62.5 μ m / 25 μ m inverter pairs distributed along its length.

For the large ring, simulations predicted a clock frequency of approximately 925 Mhz. Measurements of the actual performance vs. simulated with $V_{DD} = 2.5$ V are shown in Fig. 17. The oscillation frequency was 965 MHz. Jitter was measured at 5.5 ps RMS using a Tektronix 11801A oscilloscope with an SD-26 sampling head.

The slower than simulated rise-time discrepancy is believed to be due to the large extrinsic gate electrode resistance on the Pch FETs. At design-time, the importance of this parameter was overlooked. Transistors are now laid out according to RF design rules with the gate driven from both sides of the device.

Fig. 18 shows that the oscillation frequency F_{osc} vs. V_{DD} is quite flat over a large V_{DD} . We calculate from the measured slope that $PSRR$ is approximately 34 dB for oscillators fabricated on

this process. The oscillator was seen to be functional down to 0.8 V supply voltage, although 1.1 V was required to initiate start-up.

The test chip incorporates 15 pF of on-chip decoupling capacitance per ring. No off-chip decoupling was required. Effectively, the equivalent of ten single-ended lines each having $<10\ \Omega$ impedance were active but simultaneous switching surges are low because of the distributed switching times of the inverters.

The quad of inner rings each have the characteristics: Conductors: Width = 20 μm , Pitch = 40 μm , Ring Length = 3200 μm . Total channel widths are 2000 μm for the Nch FET and 5000 μm for the Pch FET spread over 40 pairs of inverters.

Fig. 19 shows the measured waveform from one of the 3.4 GHz rings. The oscillation frequency is 3.38 GHz vs. a simulated frequency of 3.42 GHz. However, the waveshape is disappointingly distorted, the amplitude is low, and even-mode artifacts are visible.

Investigation of the fault identified a 'co-parallel' (0°) inductive coupling problem between the clock signal lines and V_{DD} , V_{ss} supply traces running directly beneath on M3 for the complete loop length. Only when a complete FASTHENRY analysis was performed including these power traces was it apparent that induced current loops (circulating through the decoupling capacitors) were strongly attenuating the rotary signal. In this condition, the latching action (Fig. 7) does not fully develop and the rings support linear-amplification of noise signals - hence the problematic multi-mode action. (This effect was much less severe on the large 965MHz ring because the V_{DD}/V_{SS} lines were much closer to the magnetically-neutral centre-line of the transmission line). The problem can be mitigated by use of 'braided' transmission lines. (as detailed in Section IV C.).

Analysis of the test chip showed that 90° coupling between M5 and the orthogonal thin M4 lines is not a significant problem, making it possible to route power and signals between regions bounded by the rotary clock structures.

VI. CONCLUSIONS AND FURTHER WORK PLANNED

This paper has described the Rotary Travelling Wave Oscillator (RTWO) and its potential application to gigahertz rate VLSI clocking. The oscillator is unique for a resonant-style LC based oscillator in that it produces square waves directly and can be hard-wired to form Rotary Oscillator Arrays (ROA). Being LC based, the oscillator is stable and jitter is low.

The formulas presented here give practical adiabatic oscillator designs suitable for VLSI fabrication. The structure and operation of RTWO is fundamentally simple and amenable to analysis. We find that agreement between simulation and measurement is good.

We need to demonstrate *skew control* (believed to be inherent); to fully establish that the simulated performance of multi-ring ROAs is realizable, and to measure susceptibility to induced high frequency noise.

Further work is planned to establish firm mathematical / analytical foundations for the prediction of both jitter and skew and to determine exact stability criteria for arrayed oscillators.

Currently, a test chip using braided transmission line design to minimise coupling and incorporating varactors to control frequency is awaiting packaging and test.

Looking to the future, our simulations predict that the oscillator scales well. On a more modern 0.18 μ m, copper process, 10.5 GHz square-wave oscillator/distributors should be realizable consuming less than 32 mA per ring using slimmer 10 μ m conductors. From simulation, RTWO also appears to be viable on SOI processes.

ACKNOWLEDGEMENTS

This work was supported by Multigig Ltd., and partially supported by the NSF under award EIA-31332. The authors also thank Paul Franzon and Michael Steer, both of North Carolina State University - for their assistance and the Raunds and British public library service.

REFERENCES

- [1] Eby G. Friedman, *High Performance Clock Distribution Networks*, Boston, USA, Kluwer Academic Publishers, 1997.
- [2] David Harris , *Skew Tolerant Circuit Design*. Morgan Kaufmann, 2000
also David Harris phd Thesis, Stanford University, February 1999.
<http://www3.hmc.edu/~harris/research/thesis.pdf>
- [3] Gill A. Pratt and John Nguyen "Distributed Synchronous Clocking" *IEEE Transactions on Parallel and Distributed Systems*, Vol. 6, No. 3, pp314- 328 March 1995
web: <http://www.cag.lcs.mit.edu/numesh/papers/published/tpds95.html>
- [4] S.Tam, S.Rusu, U.N.Desai, R.Kim, J.Zhang and I.Young, "Clock Generation and Distribution for the first IA-64 Microprocessor" *IEEE Journal of Solid-State Circuits*, Vol. 35, No.11 Nov. 2000 pp. 1545-1552

- [5] Carl. J. Anderson et al. "Physical design of a Forth-Generation POWER GHz Microprocessor" *ISSCC 2001 Digest of Technical papers* pp232-233, p451 Feb.2001
- [6] V. L. Chi, "Salphasic distribution of clock signals for synchronous systems," *IEEE Trans. on Computers*, Vol. 43, pp. 597-602, May, 1994.
- [7] Bendik Kleveland *et. al.*, "Monolithic CMOS distributed amplifier and oscillator," *ISSCC 1999 Digest of Technical Papers*, pp. 70-71, Feb. 1999.
web: <http://smirc.stanford.edu/papers/isscc99p-bendik.pdf>
- [8] W. Athas, N. Tzartzanis, L.'J.' Svensson, L. Peterson, H. Li, X. Jiang, P. Wang, and W-C. Liu, "AC-1: A Clock-Powered Microprocessor," *Proc. of the International Symposium on Low-Power Electronics and Design*, Monterey, CA, Aug 18-20, 1997.
Web: <http://www.isi.edu/acmos/people/nestoras/papers/97-08.MontereyAC1.ps>
- [9] PCT/GB00/00175 John Wood, MultiGiG Ltd, assigned.
Web: <http://www.delphion.com/cgi-bin/viewpat.cmd/WO00044093A1>
- [10] Bendik Kleveland, Thomas H. Lee, and S. Simon Wong "50-GHz Interconnect Design in Standard Silicon Technology" *IEEE MTT-S International Microwave Symposium*, Baltimore, Maryland June 7-12, 1998
web: <http://smirc.stanford.edu/papers/mtts98p-bendik.pdf>
- [11] Bendik Kleveland, Xiaoning Qi, Liam Madden 1 , Robert W. Dutton, and S. Simon Wong "Line Inductance Extraction and Modeling in a Real Chip With Power Grid" *IEEE IEDM conference*, Washington, D. C., December 1999,
web: <http://www.gloworm.stanford.edu/tcad/pubs/device/iedm.pdf>
- [12] N.Delorme et al. "Inductance and capacitance analytic formulas for VLSI interconnect " *Electronic Letters*, 23rd May 1996, Vol.32 No.11
- [13] Charles S. Walker, *Capacitance, Inductance and Crosstalk Analysis*, Artech House, ISBN 0-89006-392-3 1990, p95
- [14] Alena Deutsch, et al, "Modeling and characterization of long on-chip interconnections for high-performance microprocessors" *IBM J. RES. DEVELOP.* VOL 39, No5, Sept. 1995 pp547-567 (p549)
- [15] James B. Beyer et al., "MESFET Distributed Amplifier Design Guidelines" *IEEE Transactions on Microwave Theory and Techniques*, VOL. MTT-32, No.3, March 1984 pp268-275
- [16] Yannis Tsividis, *Operation and Modelling of the MOS Transistor*, 2nd Edition, McGraw-Hill 1999 pp339-340
- [17] Håkan Larsson, "Distributed Synchronous Clocking using Connected Ring Oscillators"

Master's thesis in Computer Systems Engineering Centre for Computer system Architecture
Halmstad University Halmstad, Sweden, January 1997
web: <http://www.hh.se/ide/ccaweb/publications/97/distclock/9705.ps>

[18] Les Hali, Mark Clements, Wentai Liu, and Griff Bilbro, "Clock distribution using cooperative ring oscillators," *Proceedings of the 17th Conference on Advanced Research in VLSI (ARVLSI '97)*, IEEE 1997.
web: <http://www.computer.org/proceedings/arvlsi/7913/79130062abs.htm>

[19] T. C. Edwards and M. B. Steer, *Foundations of Interconnect and Microstrip Design*, Chichester, England, John Wiley & Sons, 2000, Chapter 6 section 6.11.

[20] C. Patrick Yue and S. Simon Wong, "On-Chip Spiral Inductors with Patterned Ground Shields for Si-Based RF IC's" *IEEE Journal of Solid-State Circuits*, VOL. 33, NO. 5, MAY 1998 pp 743-752
web: <http://smirc.stanford.edu/papers/JSSC98MAY-cpyue.pdf>

[21] C. P. Yue and S. S. Wong, "A study on substrate effects of silicon-based RF passive components," *1999 MTT-S International Microwave Symposium Digest*, pp 1625-1628, June 1999.
web: <http://marco.stanford.edu/swong/publications/paper73.pdf>

[22] Matthew E. Becker and Thomas F. Knight, Jr. "Transmission Line Clock Driver" *Proceedings of the 1999 IEEE International Conference on Computer Design*.
web: <http://www.computer.org/proceedings/iccd/0406/04060489abs.htm>

[23] P. Zarkesh-Ha and J.D. Meindl, "Asymptotically Zero Power Dissipation Gigahertz Clock Distribution Networks," *IEEE Electrical Performance and Electronic Packaging*, pp. 57-60, Oct. 1999
web: <http://users.ece.gatech.edu/payman/epep99.pdf>

[24] Kerry Bernstein, Keith Carrig, Christopher M. Durham and P. A. Hansen, *High Speed CMOS Design Styles*, Kulwer Academic Publishers, p22, 1998,

[25] Theerachet Soorapanth, C. Patrick Yue, Derek Shaeffer, Thomas H. Lee and S. Simon Wong "Analysis and Optimization of Accumulation-Mode Varactor for RF Ics" *Symposium on VLSI Circuits, June 11-13, 1998, Honolulu, Hawaii*
web: <http://smirc.stanford.edu/papers/VLSI98p-chet.pdf>

[26] H.B.Bakoglu, J.T.Walker, J.D.Meindl, "A symmetric Clock-Distribution Tree and Optimised High Speed Interconnections for Reduced Clock Skew in ULSI and WSI circuits" *IEEE Int'l Conf. Computer Design*, pp118-122 Oct. 1986.

[27] Matthias Bußmann and Ulrich Langmann, "Active compensation of interconnect losses for multi-GHz clock distribution networks" *IEEE Trans. on Circuits and Systems.-II: Analog and Digital Signal Processing*, Vol.39, No.11, pp 790-798, Nov. 1992

- [28] M.C. Papaefthymiou and K.H. Randall, "Edge-Triggering vs. Two-Phase Level-Clocking" *Research on Integrated Systems: Proceedings of the 1993 Symposium*, March 1993
web: <http://www.eecs.umich.edu/~marios/papers/sis93.ps>
- [29] Luca Benni et al., "Clock Skew Optimization for Peak Current Reduction", *Journal VLSI Signal Processing* 16, pp117-130 (1997)
- [30] The International Semiconductor Roadmap for Semiconductors, 1999. p41,42
web: http://public.itrs.net/files/1999_SIA_Roadmap/Design.pdf p11, p12.
- [31] Ivan S. Kourtev and Eby G. Friedman, *Timing Optimization through Clock Skew Scheduling*, Boston, USA, Kluwer Academic Publishers, 2000.
- [32] <http://www.multigig.com/software.htm>
- [33] Mattan Kamon, Michael J. Tsuk, and Jacob K. White, "FASTHENRY: a multipole-accelerated 3-D inductance extraction program," *IEEE Trans. on Microwave Theory and Techniques*, Vol. 42, pp. 1750-1758, Sept. 1994.
web: <ftp://rle-vlsi.mit.edu/pub/fasthenry/mtt.ps.Z>
- [34] The BSIM4 short-channel transistor model. University of California, Berkeley
web: <http://www-device.eecs.berkeley.edu/~bsim3/bsim4.html>



John Wood is the Engineering Director of Multigig Ltd, a U.K. technology startup specializing in multi-gigahertz rate circuit design I.P.

Previously John has worked as a consultant design engineer on multi-domain design projects in mechanical, power electronics, infrared optics and software development roles. John holds a number of patents which have been licenced for manufacture in the fields of infrared plastic welding and high speed digital signalling.

His technical interests include all areas of engineering design but particularly electromagnetics, VLSI circuit design and high speed analogue techniques.



Terence C. Edwards (M'89) received the M.Phil degree in Microwaves. He is the Executive Director of Engalco, a consultancy firm based in the U.K., mainly specialising in signal transmission technologies and the global RF and microwave industr. He researchers and takes responsibility for regular releases of Microwaves North America, published 1995,1998 and 2001. He has authored several publications (including papers published in the IEEE TRANSACTIONS ON MICROWAVE THEORY AND TECHNIQUES), has led management seminars on fiber optics, presented a paper on mobile technologies at the IMAPS Microelectronics Symposium, Philadelphia, PA, October 1997, and has written many articles and books. These include (jointly with Prof. Michael Steer) one recently in MICs (New York: Wiley) and on gigahertz and terahertz technologies (Norwood, MA: Artech, 2000). He is on the editorial advisory board for the *International Journal of Communication Systems*. He regularly consults for both national and overseas companies and is in the prestigious IEE (London) President's List of Consultants.

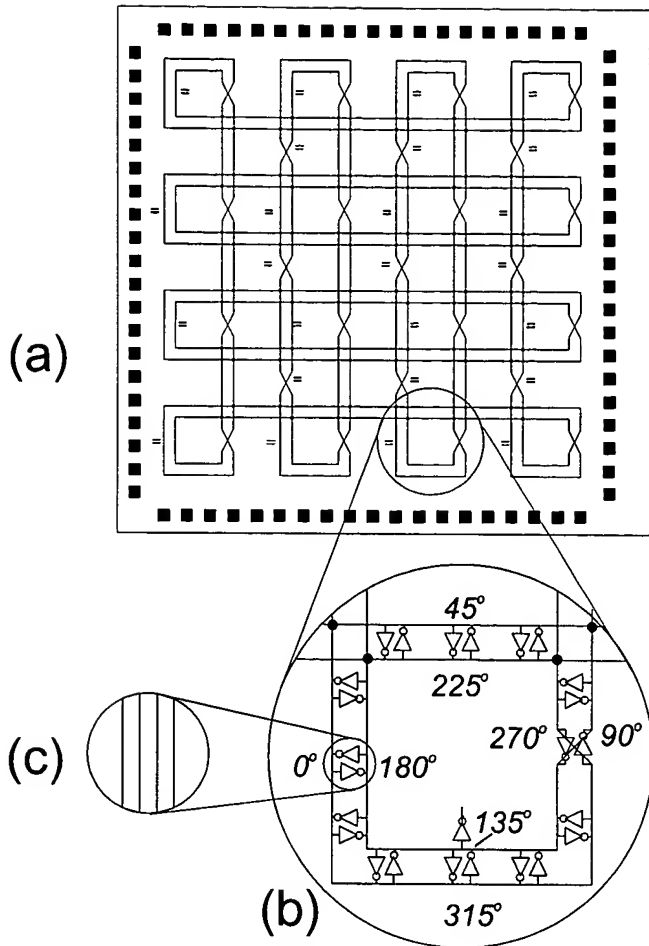
Mr Edwards is a Fellow of the Institution of Electrical Engineers (IEE), UK.



Steve Lipa (S'00) received the B.S. Degree in electrical engineering from the University of Virginia, Charlottesville in 1980, and the M.S. degree from North Carolina State University, Rayleigh, in 1993. He is currently working toward the Ph.D. degree in electrical engineering at North Carolina State University.

He is currently a Research Assistant and Laboratory Manager with the Microelectronics Systems Laboratory at North Carolina State University. He has ten years of experience as an Integrated Circuit Design Engineer, primarily in the design of high-speed digital logic circuits. His current research is in the area of high-speed clock distribution.

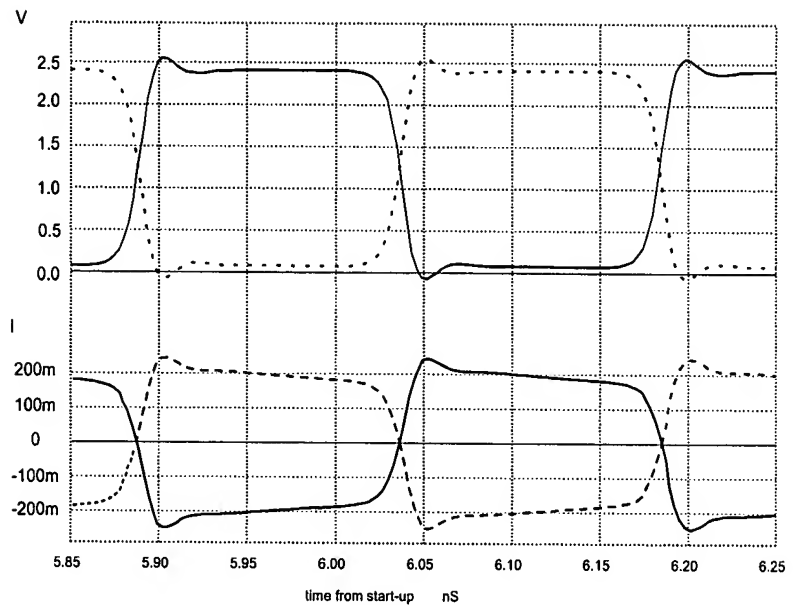
FIG1



Basic rotary clock architecture.
The = signs denote points with
same phase.

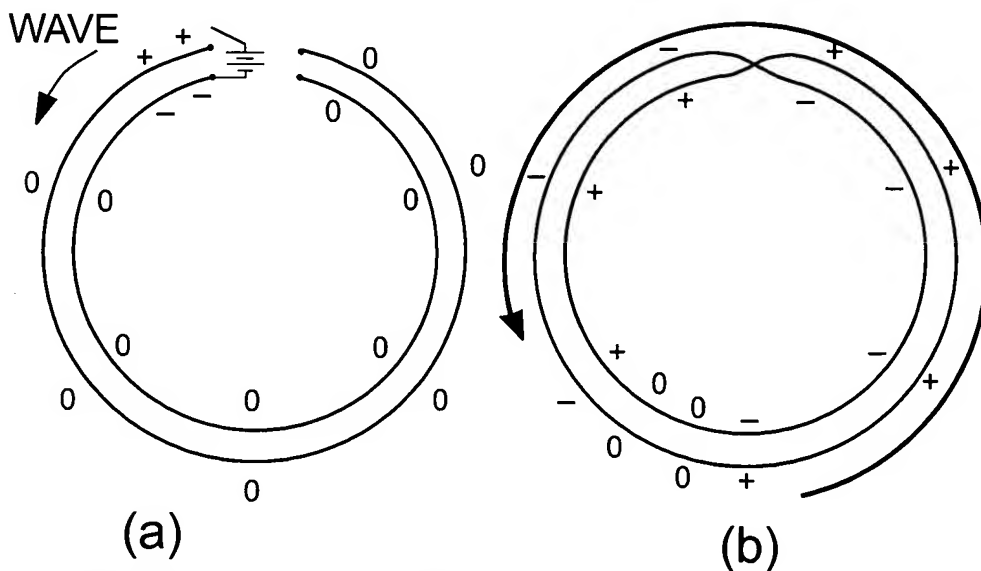
— A0 --- B0 — A0#branch --- B0#branch

FIG3



Waveforms of Line Voltage and Line Current for
the 3.4 GHz clock simulation example.

FIG2

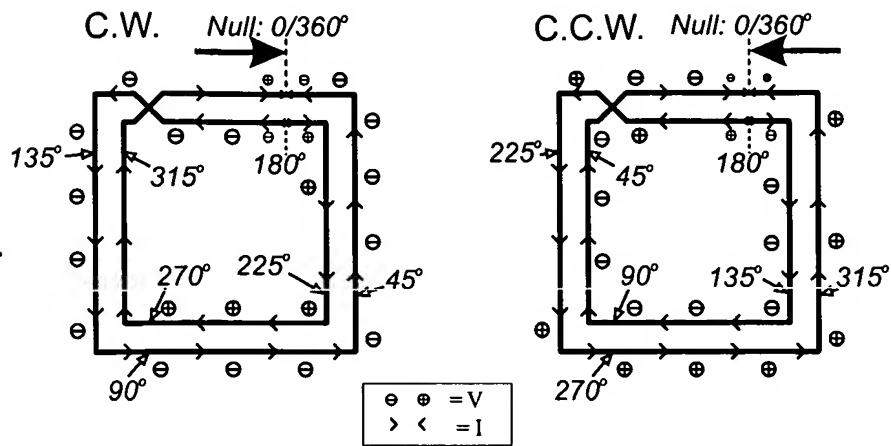


Idealized theory underlying the RTWO:

(a) open loop of differential conductors connected to a battery via a switch.

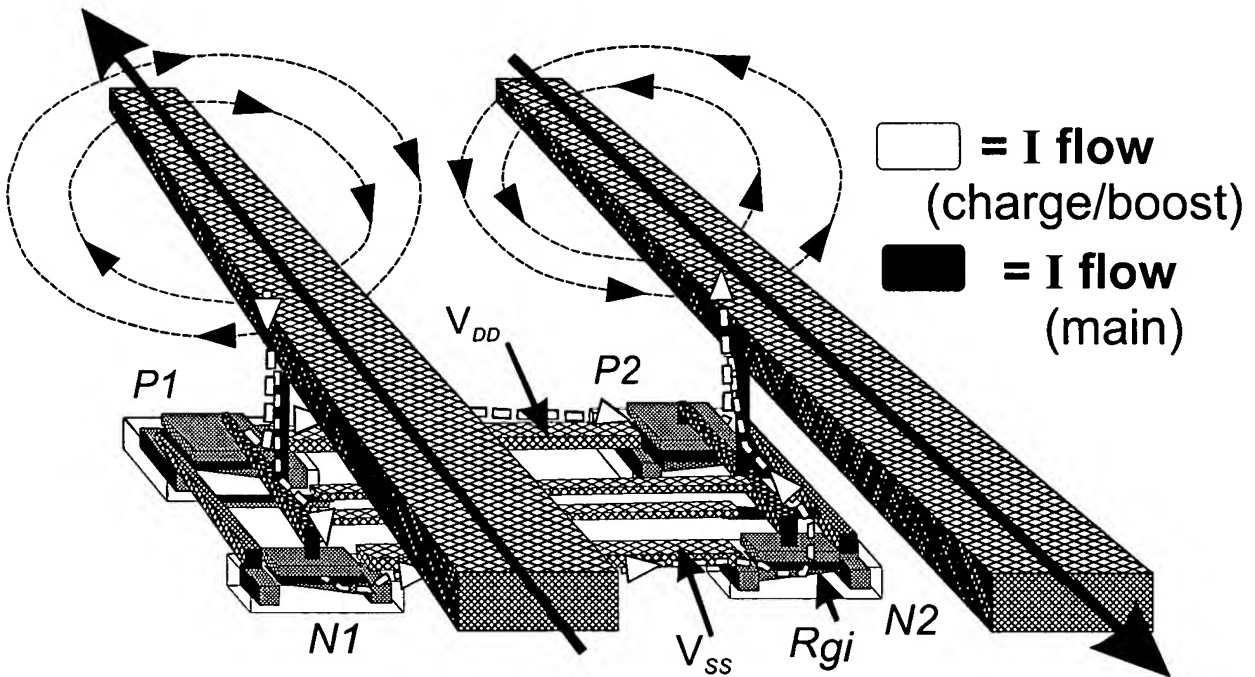
(b) similar loop but with the voltage source replaced by the inner and outer conductors cross-connected.

FIG4



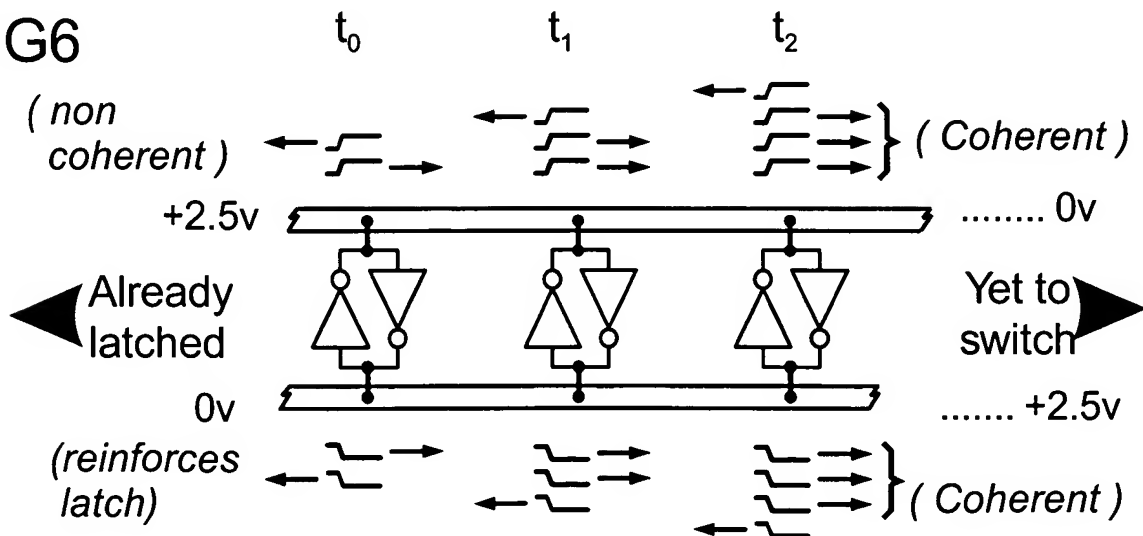
Voltage, Current and Phase relationships vs. rotation direction (Poyntings Vector)

FIG5



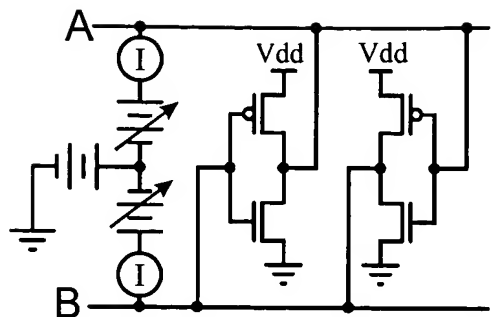
Three-dimensional view of the structure. The two differential lines are shown, with current flow arrows (main- and charge/boost) and encircling H-fields.
CMOS transistors are also shown complete with supply voltages (V_{DD} and V_{DD}) and both P and N-channels

FIG6



Expanded view of short sections of the transmission line including three sets of back-to-back inverters as a wavefront passes

FIG7



DC Transfer characteristic of two back-back inverters to an imposed differential signal

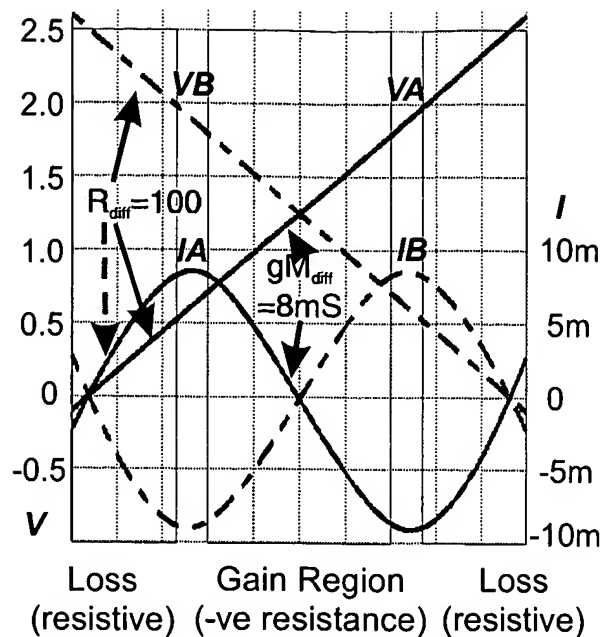
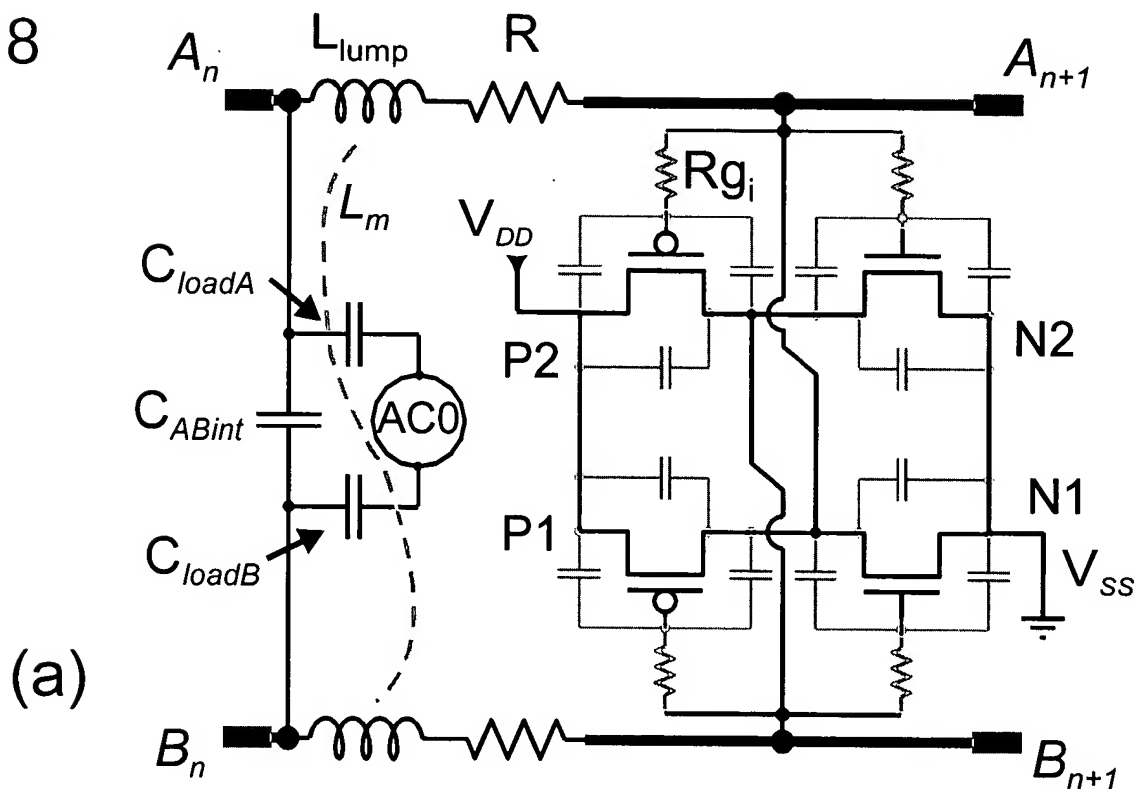
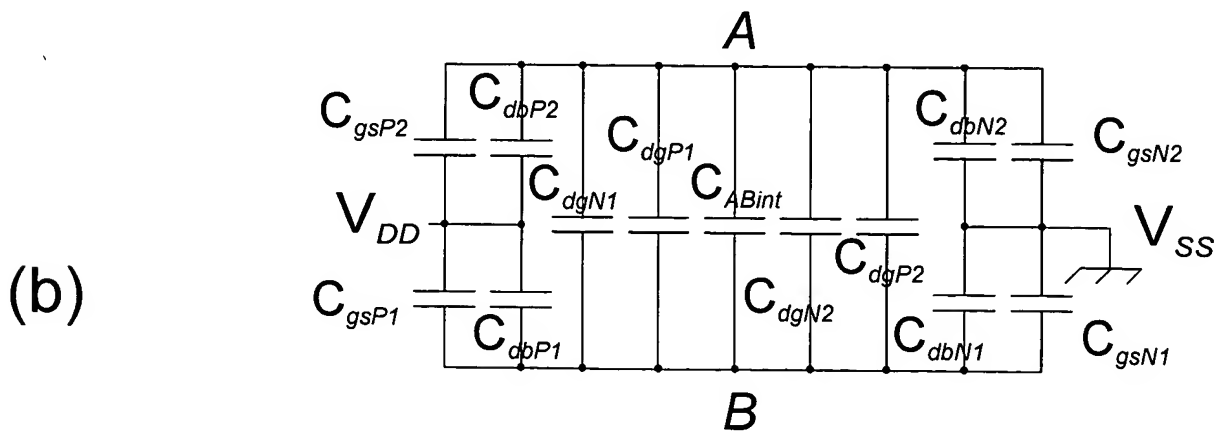


FIG8



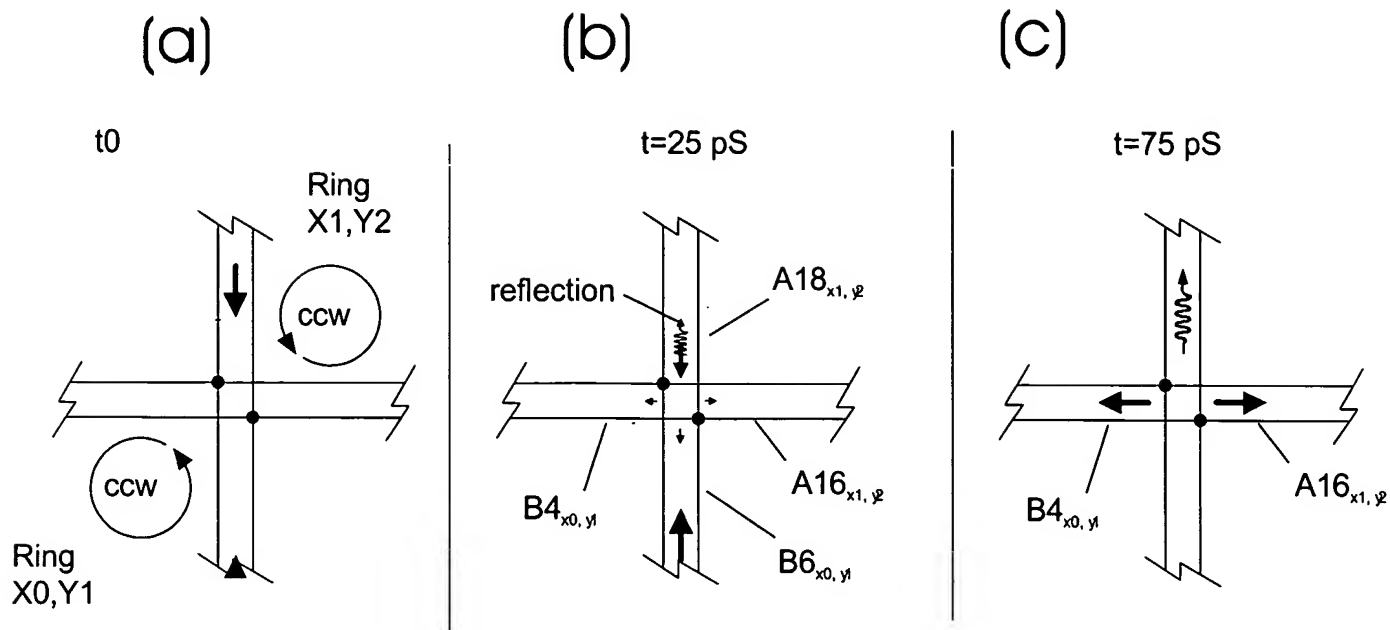
(a)



(b)

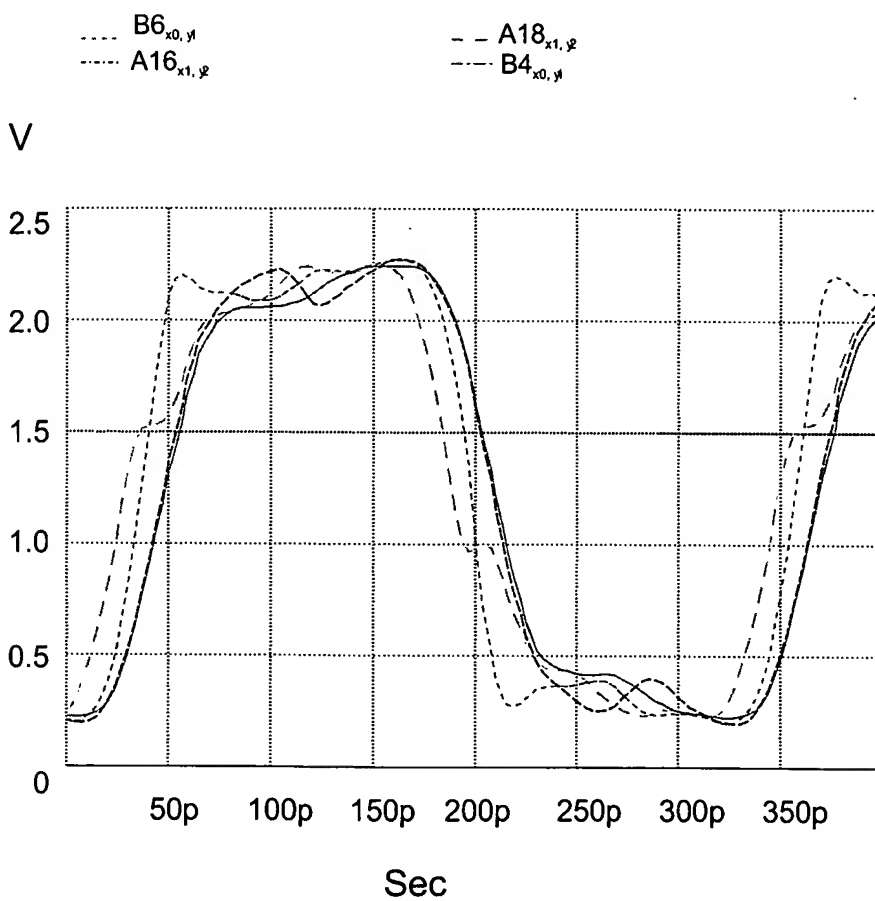
Development of the rotary clock model: (a) RF circuit adiabatic limits.
(b) capacitors replacing the transistor capacitances

FIG9



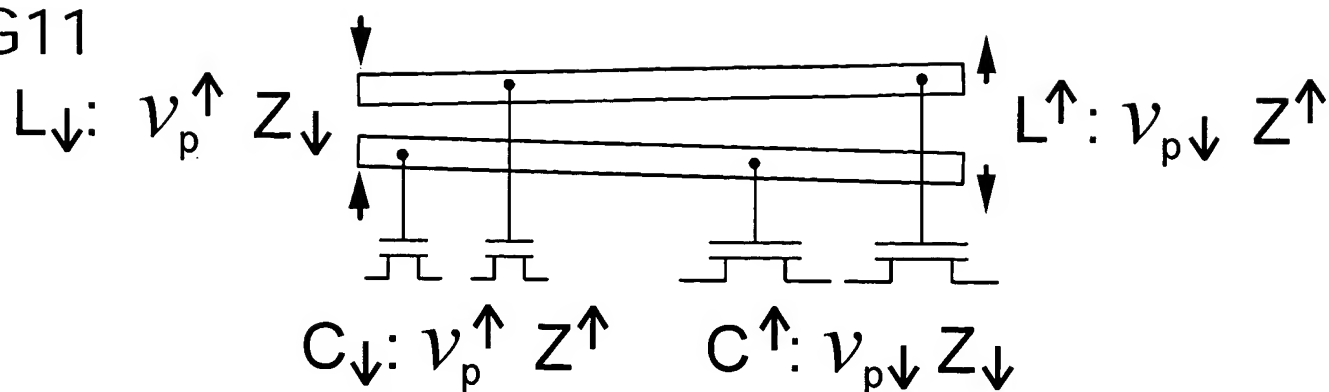
A four-port junction of two RTWO rings carrying anticlockwise signals: with a non-coincident signal arrival time

FIG10



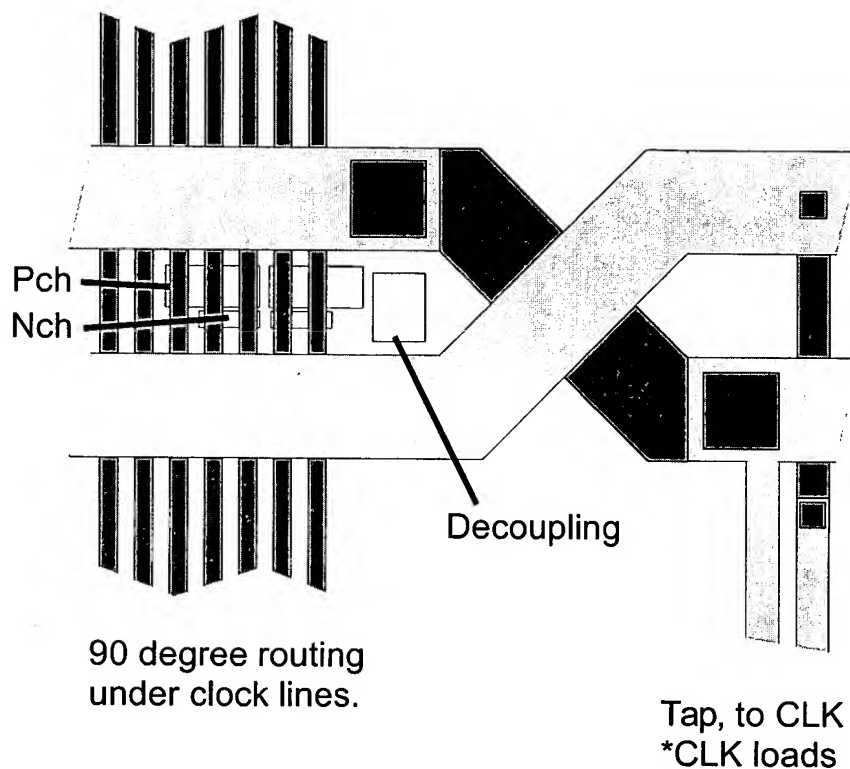
Waveforms corresponding with Fig.9

FIG11



Differential line with varying trace separations and capacitive inverter loadings indicating the effects of altering several parameters

FIG12

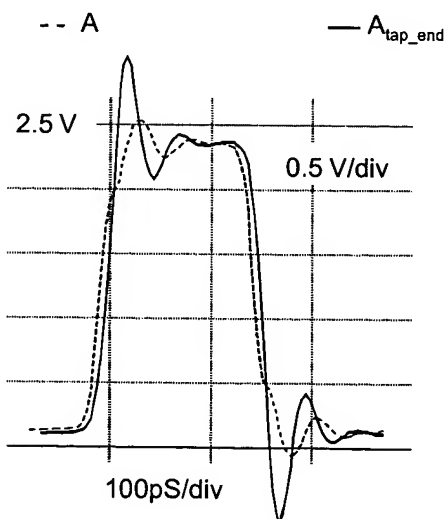


90 degree routing under clock lines.

Tap, to CLK
*CLK loads

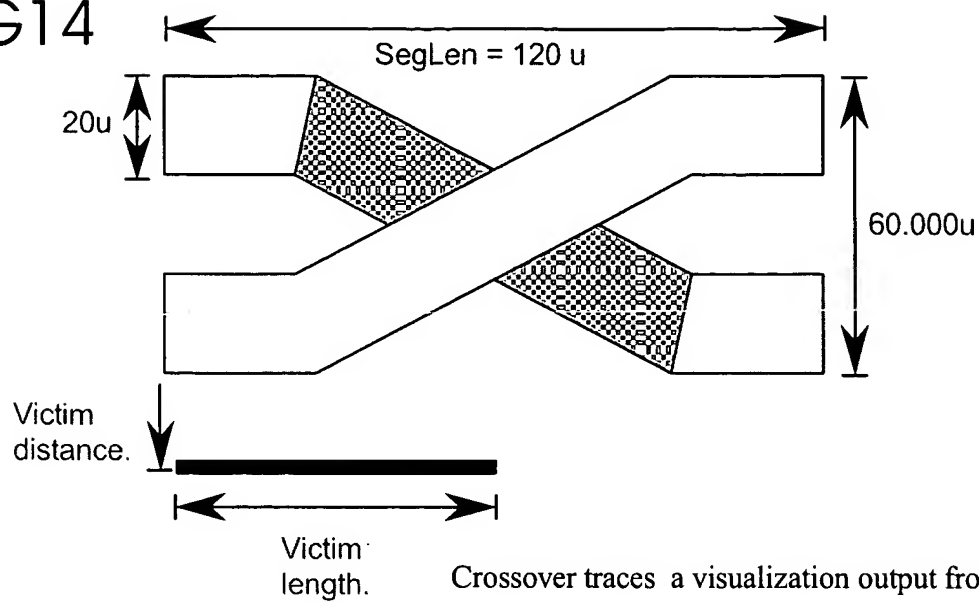
Segment of chip layout showing 90° routing beneath clock lines and a tap to clock (CLK. *CLK) loads

FIG13



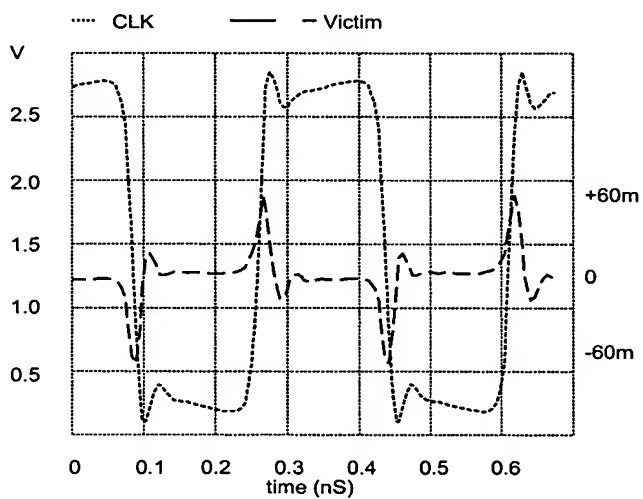
Signal at either end of a 2pF total tap loading line

FIG14



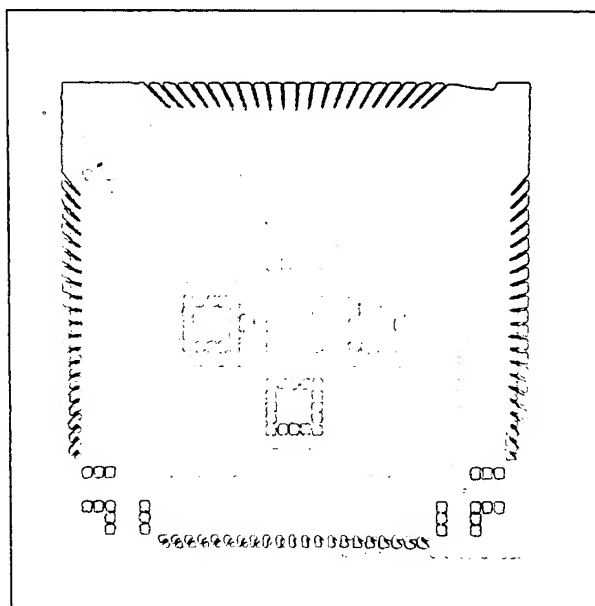
Crossover traces a visualization output from the Rotary Explorer tool

FIG15



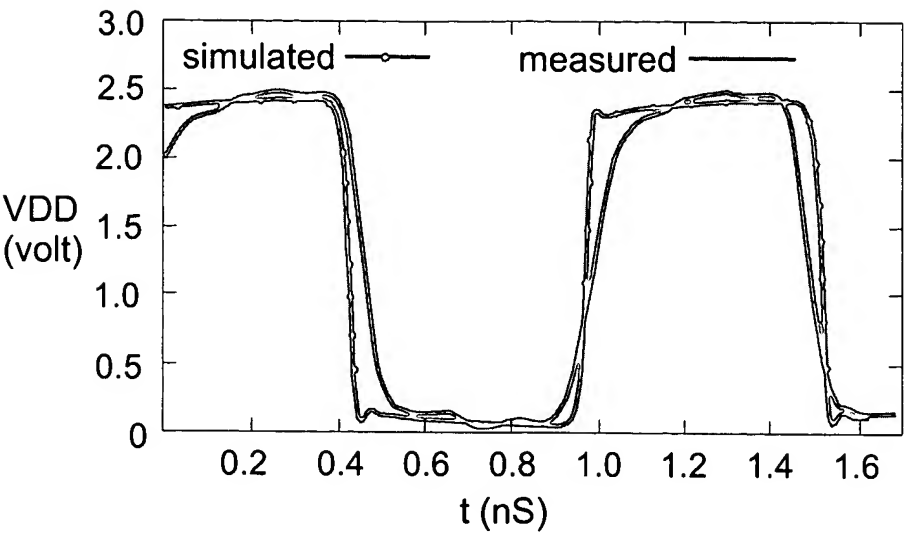
example of a notably strong coupled signal waveform

FIG16



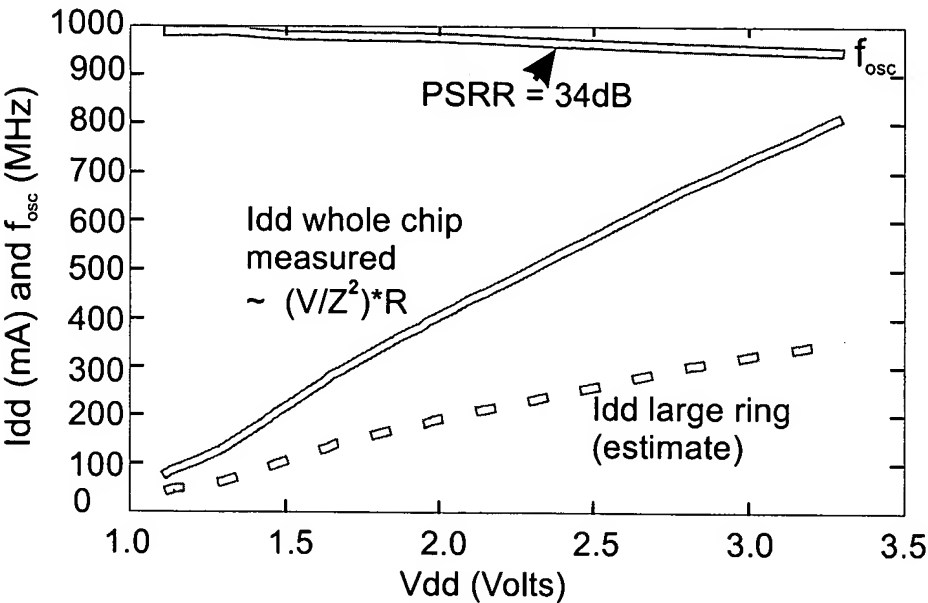
Die photograph of a prototype chip

FIG17



Measurement vs. simulation waveforms for the large 965Mhz ring.

FIG18



Clock frequency vs. VDD for the large ring and IDD vs. VDD for the entire chip with all five rings.

FIG19

